RESEARCH ARTICLE | FEBRUARY 23 2024

Natural formation of linear defect structures in MoS_2

Pavel V. Lukashev ; Timothy E. Kidd ; Haley A. Harms ; Colin Gorgen; Andrew J. Stollenwerk

Appl. Phys. Lett. 124, 083103 (2024)
https://doi.org/10.1063/5.0191536

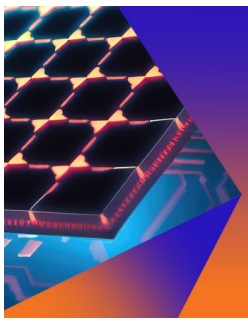

Applied Physics Letters ARTICLE pubs.aip.org/aip/apl

Natural formation of linear defect structures in MoS_2

Cite as: Appl. Phys. Lett. **124**, 083103 (2024); doi: 10.1063/5.0191536
Submitted: 14 December 2023 · Accepted: 3 February 2024 ·
Published Online: 23 February 2024

Pavel V. Lukashev, Timothy E. Kidd, Haley A. Harms, Colin Gorgen, and Andrew J. Stollenwerk[a)]

AFFILIATIONS

Physics Department, University of Northern Iowa, Cedar Falls, Iowa 50614, USA

[a)]**Author to whom correspondence should be addressed:** andrew.stollenwerk@uni.edu. **Tel.:** (319-273-7129)

ABSTRACT

Near surface defects can significantly impact the quality of metallic interconnects and other interfaces necessary to create device structures incorporating two-dimensional materials. Furthermore, the impact of such defects can strongly depend on their organization. In this study, we present scanning tunneling microscopy images and tunneling spectroscopy of point and linear defects near the surface of natural MoS_2. The point defects share similar structural and electronic characteristics and occur with comparable frequency as subsurface sulfur vacancies observed previously on natural MoS_2. The linear defects observed here occur less frequently than the point defects but share the same depth profile and electronic structure. These data indicate that the linear defects are actually a one-dimensional organization of subsurface sulfur vacancies. Our density functional calculations agree with this assessment in that, for sufficient local defect concentrations, it is energetically more favorable for the defects to be organized in a linear fashion rather than as clusters or even isolated single point defects. Given these measurements were taken from naturally formed MoS_2, this organization likely occurs during crystal formation. Considering the impact of one-dimensional organization on the local properties of layered materials, and the potential for them to be introduced purposefully during crystal formation, research into the formation mechanism and properties of these defects could enable new paths for defect engineering in MoS_2-based systems.

The scientific revolution based on two-dimensional materials began with the development of finite and single layer forms of graphite.[1,2] However, when it comes to exotic phenomena, there is no shortage of novel layered systems. For example, MoS_2 and its finite layer forms can be considered as the semiconducting analog for graphite/graphene, which opens up entirely new possibilities.[3] MoS_2 has been used to fabricate devices such as solar cells,[4,5] transistors,[6–8] and optoelectronic devices.[9] However, the integration of MoS_2 into an electronic device requires the careful selection of metallic contacts capable of forming either an Ohmic or rectifying interface, depending on the intended application. This is especially true when integrating finite layer forms of MoS_2.

Rectifying junctions are often desired in forming contacts and can form naturally at the metal–semiconductor interface as a Schottky barrier. In an ideal system, the Schottky barrier is simply the difference between the work function of the metal and the electron affinity of the semiconductor. In reality, the Schottky barrier is often dominated by interface defects that result in Fermi level pinning.[10,11] For example, although Au/MoS_2 is reported to exhibit rectifying properties, both *n*-type and *p*-type characteristics have been observed in seemingly similar structures.[10,12–16] In addition, the presence of defects can lead to parallel conduction at the interface, causing small areas of localized Ohmic contact even when a rectifying contact is intended.[13] This indicates that a small density of defects can dominate the electronic behavior of the interface. Therefore, a comprehensive understanding of surface and subsurface defects is essential for effective control of the electronic properties at the metal/MoS_2 interface. A number of scanning tunneling microscopy (STM) and atomic force microscopy (AFM) studies have investigated the structural and electronic properties of such defects on natural and artificially grown MoS_2.[11,13,17–21] In MoS_2, experimental and computational studies have shown that S vacancies are the most prominent surface defects.[22–24] These defects are stable[21,22] and known to affect the charge transport characteristics of MoS_2.[25,26]

There is also evidence that the particular arrangement of S vacancy defects can strongly impact system properties.[27] For example, studies have shown that linear arrangements of S vacancies could result in topological superconductivity,[28] and isolated vacancies can enhance catalytic activity.[29,30] Successful efforts have been made to engage in defect engineering. Of note are some interesting studies

performed on monolayer MoS_2. In these experiments, it was shown that a random distribution of isolated surface S vacancies spontaneously line up to form linear structures when exposed to electron radiation.[31,32] Given the constraints of chemical bonding within the interior of MoS_2, it is likely that such defect migration would be impossible for subsurface layers. However, we have found that such linear arrangements occur in natural MoS_2 and could be induced through defect engineering during crystal growth. Hence, understanding the arrangement of defects into point or linear formations could be quite useful as even subsurface S vacancies, especially located just below the surface MoS_2 layer, can have a strong impact on interfacial electronic properties.

In this paper, we explore point and linear defects occurring near the surface in natural MoS_2 crystals. Both arrangements manifest as depressions in the surface of our STM images. The dimensions and surface density of the point defects correlate with subsurface S vacancies as seen in other studies of natural MoS_2. Tunneling spectroscopy from both defects induce a similar shift in the Fermi level away from the valence band, as expected from subsurface S vacancies. Vertical displacement and differential tunneling spectra similarities suggest that the point and linear structures result from the same fundamental type of defect. Both defects can have a significant impact on the interface properties of metallic interconnects and should be considered when fabricating MoS_2-based devices. Our density functional calculations indicate that linear arrangements of subsurface S vacancies are the most energetically favorable configuration if the local concentration of the vacancies is relatively high. They also show that clustering of defects about a single point is the least favorable arrangement. These calculations correlate well with STM observation, which show that isolated vacancies are the most common defect, and vacancy clusters are never seen.

The MoS_2 samples utilized in this study were sourced from natural deposits and acquired commercially from SPI Supplies. All samples were first mechanically exfoliated in air, then transferred into a variable temperature STM (Omicron) chamber with a base of 1×10^{-10} mbar. Exposure to ambient conditions was minimal, with sample transfer times no more than five minutes. STM tips were mechanically cut from 0.25 mm diameter $Pt_{0.9}Ir_{0.1}$ wire. Differential spectra were recorded at room temperature using a lock-in amplifier with a 3.5 kHz, 2.0 V modulation. All spectra were acquired after first stabilizing the tip with a tunneling voltage of 1.0 V and a current setpoint of 1.0 nA. Spectra acquired on defects were acquired in the middle of the scan to minimize impact from piezo drift. Data analysis was performed using GWYDDION software.[33]

We performed our density function theory (DFT) calculations using the Vienna *ab initio* simulation package (VASP),[34] within the projector augmented-wave method (PAW)[35] and generalized-gradient approximation (GGA).[36] The Brillouin-zone sampling is performed with the *k*-mesh of $1 \times 1 \times 1$ for atomic relaxation and $2 \times 2 \times 1$ for electronic structure calculations. A relatively small number of *k*-points is due to a large size of the supercell—150 atoms with a vacuum layer imposed, as explained below in the text. Various S vacancy configurations are simulated by removing S atoms from the supercell and relaxing the geometry of the obtained structure. We set the energy convergence to 10^{-3} meV, and we employed the integration method by Methfessel and Paxton[37] with a cutoff energy of 500 eV. The crystal structures are visualized with the MedeA® software environment.[38] All calculations performed in this work are done using the Advanced Cyberinfrastructure Coordination Ecosystem: Services & Support (ACCESS) [formerly known as Extreme Science and Engineering Discovery Environment (XSEDE)] resources located at the Pittsburgh Supercomputing Center (PSC),[39] and with the resources of the Center for Functional Nanomaterials (CFN) at Brookhaven National Laboratory (BNL).

Large-scale images of the MoS_2 samples revealed the surface to be atomically flat with pronounced step edges spanning several micrometers. Inspection of high-resolution images show the existence of point-like defects on the surface as seen in Fig. 1(a). These point defects were found to be common at multiple locations on four different MoS_2 crystals. Images such as seen in Fig. 1(b) indicate that the point defects have a diameter of approximately 1–2 nm and a depth between 0.1 and 0.3 nm. Point defects with density and dimensions similar to ours and also prevalent on the surface have been previously observed and attributed to subsurface S vacancies.[40] In addition to point defects, linear defects were also observed as seen in Fig. 1(c). The observed defects exhibit a width ranging from 2 to 3 nm, while their depths ranged between 0.2 and 0.3 nm, similar in depth to the point defects. Linear defects were less common than the point defects, but were still observed in different locations on multiple samples. Linear defects were observed in Mn intercalated $Ti_{1+\delta}S_2$ and were attributed to the interactions and arrangement of Mn and Ti ions located within the intercalation sites.[41] It has also been shown that electron irradiation of surface S defects on MoS_2 results in linear structures, possibly due to mechanical strain in the crystal.[31,32] These results suggest that defects are prone toward linearity in 2D dichalcogenides crystals under certain circumstances.

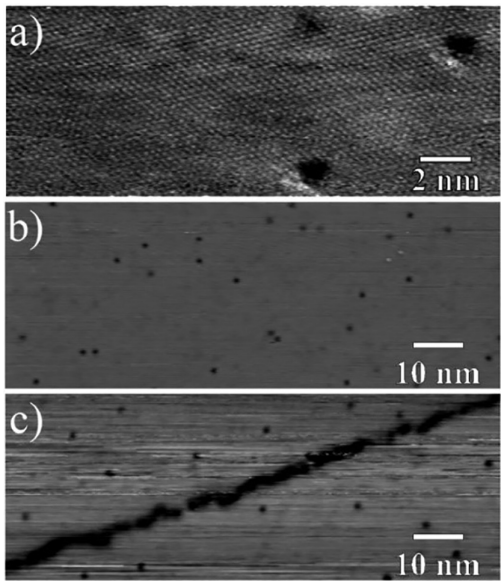

FIG. 1. (a) High-resolution STM image showing three point defects ($V_{tip} = 1.3$ V, $I_{tip} = 1.3$ nA). (b) STM image showing the typical point defect density found on as exfoliated MoS_2 ($V_{tip} = -1.2$ V, $I_{tip} = 1.0$ nA). (c) STM image showing a linear defect surrounded by point defects on as exfoliated MoS_2 ($V_{tip} = -1.5$ V, $I_{tip} = 1.0$ nA).

The two types of defects were characterized using differential spectroscopy obtained using a lock-in amplifier. Figure 2(a) shows a reference spectrum typical of those found in regions devoid of defects. These spectra have a bandgap that vary from 1.1 to 1.3 eV and all have a Fermi level that is located very close to the valence band. The spectrum obtained on point defects, exemplified in Fig. 2(b), showed a similar bandgap within the experimental uncertainty. However, the Fermi level measured on point defects is shifted away from the valence band by approximately 0.35 eV. A shift such as this could be the result of the defects behaving as a dopant site. Sulfur vacancies are known to cause an *n*-type shift away from the valence band,[42] this would be consistent with our hypothesis that point defects are caused by subsurface S vacancies. Interestingly, spectrum obtained on the linear defects exhibit a similar shift from the valence band as seen in Fig. 2(c). Given that both the depth and electronic properties of the point and 1D defects were nearly identical, it seems very likely that both point and linear defects are the result of subsurface S vacancies.

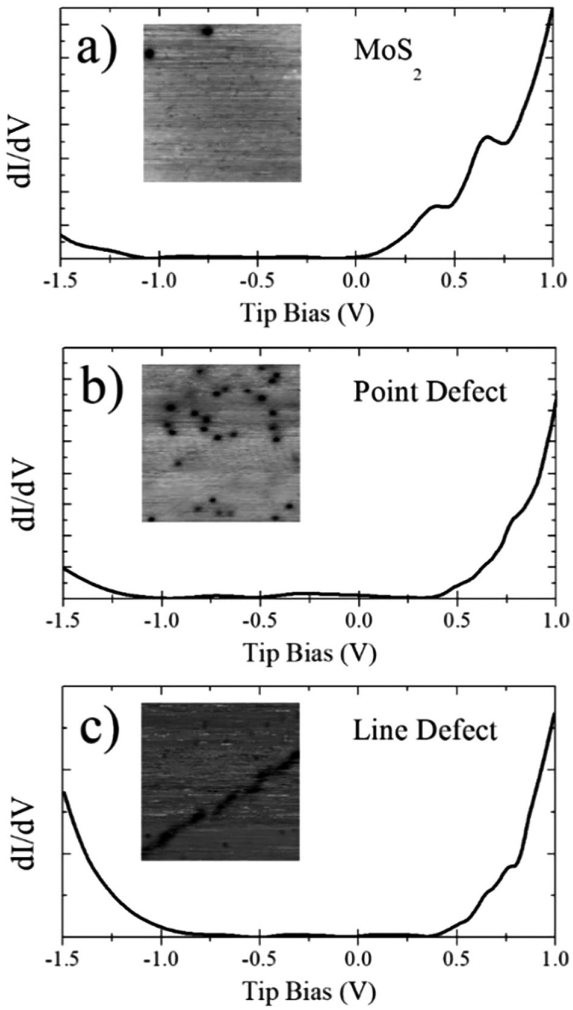

FIG. 2. Typical differential conductance spectra acquired on MoS_2 (a) in a region with no defects, (b) on a point defect, and (c) on a line defect. Each spectrum was stabilized at $V_{tip} = 1.0$ V, $I_{tip} = 0.5$ nA prior to sweeping the voltage. Inset images have dimensions of 50×50 nm^2.

To gain insight into the formation mechanism of the observed vacancies, we performed a series of DFT calculations. In particular, we constructed a bilayer of $Mo_{50}S_{100}$, i.e., a $5 \times 5 \times 2$ cell of MoS_2 [see Fig. 3 for the top view (a) and side view (b) of this cell]. We imposed a 20 Å vacuum layer in the stacking direction [z-direction in Fig. 3(b)] to avoid potential overlap of wavefunctions due to translational symmetry. Next, we calculated energies of this cell with 2, 3, and 4 S vacancies (i.e., $Mo_{50}S_{98}$, $Mo_{50}S_{97}$, and $Mo_{50}S_{96}$, correspondingly) for various configurations, which are visualized in Fig. 4, and discussed in the text below.

We considered two types of S vacancy defects: cluster and line. In the former, the vacancies are located at the nearest neighbor S sites, as shown in the top panel of Fig. 4. In the latter, the vacancies are arranged in a linear fashion, see top left, middle bottom, and right bottom images in Fig. 4. The cluster and line defects for two S vacancies ($Mo_{50}S_{98}$) are obviously identical (top left image in Fig. 4). Along with cluster and line arrangements, we also considered point-like defects for all three considered cells: $Mo_{50}S_{98}$, $Mo_{50}S_{97}$, and $Mo_{50}S_{96}$. Here, the vacancies are arranged in more or less random way, as long as they exclude nearest neighbor vacancies. Bottom left image in Fig. 4 illustrates such arrangement for $Mo_{50}S_{96}$ ($Mo_{50}S_{98}$ and $Mo_{50}S_{97}$ cells are arranged in a similar way). To verify that exclusion of the nearest neighbor vacancies is sufficient to simulate point defects (i.e., next nearest neighbors may be included), we performed additional calculations. In particular, we removed a single S atom from the cell and analyzed the change in the positions of the remaining S atoms in the layer from which the S atom was removed after structural optimization. Our calculations indicate that the S atoms neighboring the vacancy get closer to the vacancy by about 0.1 Å. At the same time, the *next nearest neighbors* are virtually unaffected by the presence of the vacancy (i.e., they do not "move" upon atomic relaxation). Thus, we conclude that to simulate the point-like S vacancies, one only needs to exclude the nearest neighbor vacancies from the cell.

For all the configurations discussed in the previous paragraph, we considered vacancies formed at both the surface and the subsurface of the MoS_2 bilayer. This is done by removing S atoms from the first (surface) and third (subsurface) atomic layers of S shown in Fig. 3(b). The geometry of all considered configurations were fully optimized, and the total energy subsequently calculated. Figure 5 summarized the results of our calculations, as discussed below.

Figure 5 shows $E_{line/cluster} - E_{point}$ for all four considered cases. Here, $E_{line/cluster}$ and E_{point} indicate calculated energies of line/cluster and point defects, correspondingly. The negative energy difference indicates the line/cluster configuration being energetically more

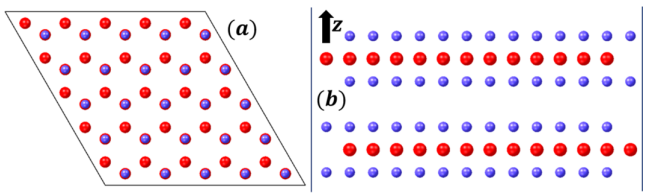

FIG. 3. Top view (a) and side view (b) of $5 \times 5 \times 2$ cell of MoS_2. Red spheres—Mo, blue spheres—S. A 20 Å vacuum layer in the stacking direction [z-direction in Fig. 3(b)] is imposed.

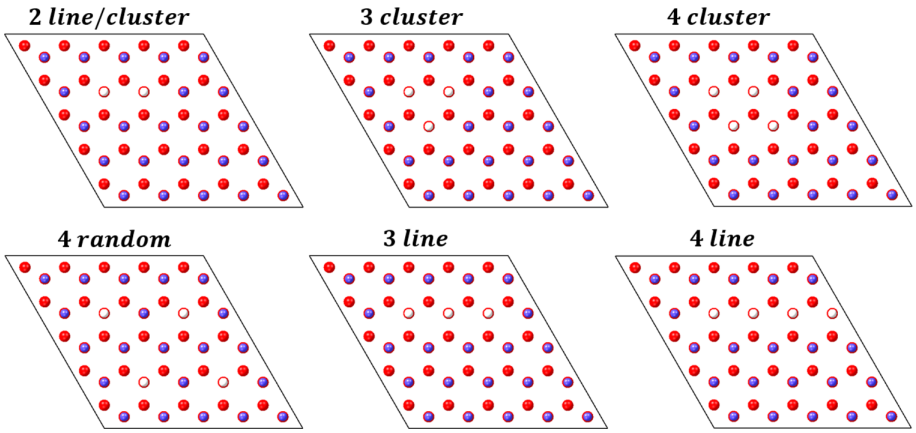

FIG. 4. Types of S vacancy configurations considered in this work. The missing S atoms can be seen as white spheres surrounded by red circles (which are Mo atoms behind the S vacancies).

favorable than point defects. As seen in the figure, all considered cluster defect configurations are energetically unfavorable compared with point defects. At the same time, line defects are energetically favorable over point defects from the 3 and 4 S vacancies. As mentioned above, the configuration with 2 S vacancies may be treated as both line and cluster, but the latter is probably more appropriate. In any case, for two vacancies, the calculated energy differences are very small (slightly positive). Another interesting feature shown in Figure 5 is that for line defects, the subsurface vacancies are energetically more favorable than surface vacancies. In addition, increasing the number of S line vacancies increases the absolute value of the energy difference, seemingly indicating that the line defects are becoming more energetically favorable. All these results may be summarized in statements presented in the following paragraph.

Results presented in Fig. 5 clearly indicate that line defects are energetically more favorable compared with point defects of S vacancies. It is also seen that the cluster defects are not energetically

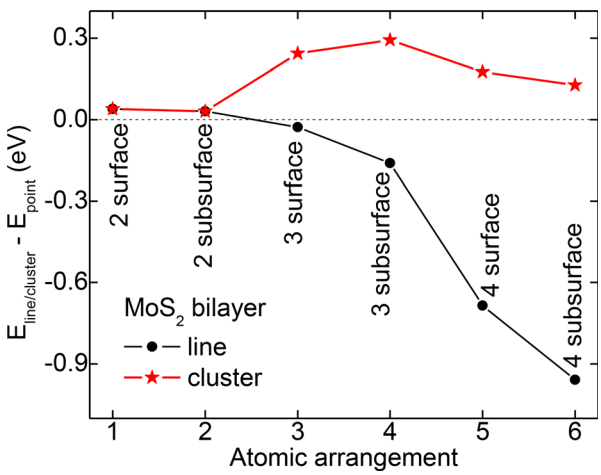

FIG. 5. Calculated energy differences for the considered systems with S vacancies. The negative energy difference indicates the nearest neighbor vacancies being energetically more favorable than point defects. The number of removed S atoms is indicated in the figure, e.g., "3 surface" means 3 S atoms removed from the surface, while e.g., "2 subsurface" means 2 S atoms removed from the subsurface.

favorable compared with the point defects. The figure also clearly indicates that subsurface vacancies are energetically favorable compared with surface vacancies in line defects. Thus, it seems plausible to conclude that if the number of S vacancies is low, we will likely see point defects only (purely by statistical arguments). However, if the concentration of vacancies increases, they can (again, statistically speaking), in principle, congregate in two types of defects—cluster and line. However, our calculations indicate that cluster defects are significantly less likely than line defects. These results appear to be in agreement with the distribution of the defects observed in our samples.

In addition to the arguments presented earlier, other physical mechanisms should be considered, such as sample imperfection and effect of temperature. These kinds of studies go beyond the standard density functional calculations, but we hope that other techniques in future studies may shed more light on the nature of the observed linear defects. In addition, it is not unreasonable to assume that the two types of subsurface defects (point and linear) are driven by separate mechanisms. For example, the formation process of the natural MoS_2 may generally favor a disordered arrangement of subsurface S vacancies, resulting in the large number of isolated defects seen randomly distributed on the surface in numerous studies. The linear structures may only form along grain boundaries or as a result of localized strain. Control over such local conditions could be possible during the formation of MoS_2, for example, in growing finite layers upon a templated surface. If the impact on properties is desirable enough, defect engineering techniques should be able to produce the energetically favorable linear arrangements seen here. In addition, our calculations indicate that the presence of S vacancies does not result in induced magnetism in the system. Figure S1 (see supplement material) demonstrates this for the case of four atomic S vacancies. As seen from the figure, the presence of defects results in additional states in the energy gap; however, the system is still non-spin-polarized. This allows us to cautiously rule out the presence of uncompensated spins induced by the S vacancies.

Our STM measurements demonstrate that the surface of natural MoS_2 exhibits a high density of point defects and also a significant number of linear defect structures. The structural and electronic properties of both defect types are very similar as measured by STM, indicating they share a common origin. Previous studies of point defects on natural MoS_2 suggest they both arise due to subsurface S vacancies. Our DFT calculations on different types of vacancy arrangements show that the linear

arrangements of subsurface S vacancies are the most energetically favorable configuration for relatively larger concentration of vacancies. These results, in conjunction with the potential emergent phenomena associated with linear defect arrangements, show future research into defect engineering could strongly impact our understanding of dimensional confinement and interface properties for MoS_2-based systems. Future experiments should grow MoS_2 under different conditions to better understand the formation mechanism of the linear defects. For example, growth could occur while applying stress to the crystal to see if the point defects congregate toward the stressed region. In order to better understand the formation mechanism of these linear defects, one can explore the relationship between defect type and density with single crystal growth parameters such as the initial stoichiometry, thermal gradient, annealing temperature, and thermal ramping. For example, slower growth rates can be used to minimize strain, metal dopants could change the local bonding environments, and variations of initial sulfur content would determine the density of sulfur vacancy defects. Furthermore, one could explore film growth in finite layer MoS_2 systems where strain can also be influenced by the choice of the growth substrate.

See the supplementary material for Fig. S1 that shows the calculated total density of states of the bilayer MoS_2 with and without S vacancies. As shown in the figure, the bilayer MoS_2 retains its semiconducting non-spin-polarized character in the presence of all the arrangements of S vacancies considered in this work.

P.V.L. and T.E.K. were supported by the U.S. Department of Energy, Office of Science (Grant No. DE-SC0020334). A.J.S. was supported by the National Science Foundation (Grant No. DMR-2300639). This work used the Advanced Cyberinfrastructure Coordination Ecosystem: Services & Support (ACCESS) [formerly known as Extreme Science and Engineering Discovery Environment (XSEDE)], which is supported by the National Science Foundation, Grant No. ACI-1548562. This work used the XSEDE Regular Memory (Bridges 2) and Storage (Bridges Ocean) at the Pittsburgh Supercomputing Center (PSC) through allocation No. TG-DMR180059 and the resources of the Center for Functional Nanomaterials, which is a U.S. DOE Office of Science Facility, and the Scientific Data and Computing Center, a component of the Computational Science Initiative, at Brookhaven National Laboratory (BNL) under Contract No. DE-SC0012704.

AUTHOR DECLARATIONS

Conflict of Interest

The authors have no conflicts to disclose.

Author Contributions

Pavel V. Lukashev: Data curation (equal); Formal analysis (equal); Funding acquisition (equal); Investigation (equal); Software (equal); Visualization (equal); Writing – original draft (equal); Writing – review & editing (equal). **Timothy E. Kidd:** Formal analysis (supporting); Funding acquisition (equal); Resources (equal); Validation (equal); Writing – review & editing (equal). **Haley A. Harms:** Data curation (equal); Formal analysis (equal); Investigation (equal); Visualization (equal). **Colin Gorgen:** Data curation (equal); Investigation (equal). **Andrew J. Stollenwerk:** Conceptualization (equal); Data curation (equal); Formal analysis (equal); Funding acquisition (equal); Supervision (equal); Writing – original draft (equal).

DATA AVAILABILITY

The data that support the findings of this study are available from the corresponding author upon reasonable request.

REFERENCES

[1]K. S. Novoselov, A. K. Geim, S. V. Morozov, D. Jiang, M. I. Katsnelson, I. V. Grigorieva, S. V. Dubonos, and A. A. Firsov, "Two-dimensional gas of massless Dirac fermions in graphene," Nature **438**, 197 (2005).
[2]Y. Zhang, Y.-W. Tan, H. L. Stormer, and P. Kim, "Experimental observation of the quantum Hall effect and Berry's phase in graphene," Nature **438**, 201 (2005).
[3]K. F. Mak, C. Lee, J. Hone, J. Shan, and T. F. Heinz, "Atomically thin MoS_2: A new direct-gap semiconductor," Phys. Rev. Lett. **105**, 136805 (2010).
[4]Y. Zhao and G. Ouyang, "Thickness-dependent photoelectric properties of MoS_2/Si heterostructure solar cells," Sci. Rep. **9**, 17381 (2019).
[5]S. Rashidi, S. Rashidi, R. K. Heydari, S. Esmaeili, N. Tran, D. Thangi, and W. Wei, "WS_2 and MoS_2 counter electrode materials for dye-sensitized solar cells," Prog. Photovoltaics **29**, 238 (2021).
[6]B. Radisavljevic, A. Radenovic, J. Brivio, V. Giacometti, and A. Kis, "Single-layer MoS_2 transistors," Nat. Nanotechnol. **6**, 147 (2011).
[7]S. Kim, A. Konar, W. Hwang, J. Lee, J. Lee, J. Yang, C. Jung, H. Kim, J. Yoo, J. Choi, Y. Jin, S. Lee, D. Jena, W. Choi, and K. Kim, "High-mobility and low-power thin-film transistors based on multilayer MoS_2 crystals," Nat. Commun. **3**, 1011 (2012).
[8]N. Liu, J. Baek, S. M. Kim, S. Hong, Y. K. Hong, Y. S. Kim, H.-S. Kim, S. Kim, and J. Park, "Improving the stability of high-performance multilayer MoS_2 field-effect transistors," ACS Appl. Mater. Interfaces **9**, 42943 (2017).
[9]M. Amani, D. Lien, D. Kiriya, J. Xiao, A. Azcatl, J. Noh, S. R. Madhvapathy, R. Addou, S. Kc, M. Dubey, K. Cho, R. M. Wallace, S. Lee, J. He, J. W. Ager III, X. Zhang, E. Yablonovitch, and A. Javey, "Near-unity photoluminescence quantum yield in MoS_2," Science **350**, 1065 (2015).
[10]M. Cook, R. Palandech, K. Doore, Z. Ye, G. Ye, R. He, and A. J. Stollenwerk, "Influence of interface coupling on the electronic properties of the Au/MoS_2 junction," Phys. Rev. B **92**, 201302 (2015).
[11]P. Bampoulis, R. van Bremen, Q. Yao, B. Poelsema, H. J. W. Zandvliet, and K. Sotthewes, "Defect dominated charge transport and fermi level pinning in MoS_2/metal contacts," ACS Appl. Mater. Interfaces **9**, 19278 (2017).
[12]W. Mönch, "Valence-band offsets and Schottky barrier heights of layered semiconductors explained by interface-induced gap states," Appl. Phys. Lett. **72**, 1899 (1998).
[13]S. McDonnell, R. Addou, C. Buie, R. M. Wallace, and C. L. Hinkle, "Defect-dominated doping and contact resistance in MoS_2," ACS Nano **8**, 2880 (2014).
[14]N. Kaushik, A. Nipane, F. Basheer, S. Dubey, S. Grover, M. M. Deshmukh, and S. Lodha, "Schottky barrier heights for Au and Pd contacts to MoS_2," Appl. Phys. Lett. **105**(11), 113505 (2014).
[15]C. Maurel, F. Ajustron, R. Péchou, G. Seine, and R. Coratger, "Electrical behavior of the Au/MoS_2 interface studied by light emission induced by scanning tunneling microscopy," Surf. Sci. **600**, 442 (2006).
[16]C. Maurel, R. Coratger, F. Ajustron, J. Beauvillain, and P. Gerard, "Electrical characteristics of metal/semiconductor nanocontacts using light emission in a scanning tunneling microscope," J. Appl. Phys. **94**, 1979 (2003).
[17]R. Addou, L. Colombo, and R. M. Wallace, "Surface defects on natural MoS_2," ACS Appl. Mater. Interfaces **7**, 11921 (2015).
[18]W. Lu, B. Birmingham, and Z. Zhang, "Defect engineering on MoS_2 surface with argon ion bombardments and thermal annealing," Appl. Surf. Sci. **532**, 147461 (2020).
[19]P. Vancsó, G. Z. Magda, J. Pető, J.-Y. Noh, Y.-S. Kim, C. Hwang, L. P. Biró, and L. Tapasztó, "The intrinsic defect structure of exfoliated MoS_2 single layers revealed by scanning tunneling microscopy," Sci. Rep. **6**, 29726 (2016).
[20]S. Najmaei, Z. Liu, W. Zhou, X. Zou, G. Shi, S. Lei, B. I. Yakobson, J.-C. Idrobo, P. M. Ajayan, and J. Lou, "Vapour phase growth and grain boundary structure of molybdenum disulphide atomic layers," Nat. Mater. **12**, 754 (2013).

[21]D. Liu, Y. Guo, L. Fang, and J. Robertson, "Sulfur vacancies in monolayer MoS_2 and its electrical contacts," Appl. Phys. Lett. **103**, 183113 (2013).
[22]W. Zhou, X. Zou, S. Najmaei, Z. Liu, Y. Shi, J. Kong, J. Lou, P. M. Ajayan, B. I. Yakobson, and J.-C. Idrobo, "Intrinsic structural defects in monolayer molybdenum disulfide," Nano Lett. **13**, 2615 (2013).
[23]J.-Y. Noh, H. Kim, and Y.-S. Kim, "Stability and electronic structures of native defects in single-layer MoS_2," Phys. Rev. B **89**, 205417 (2014).
[24]H.-P. Komsa and A. V. Krasheninnikov, "Native defects in bulk and monolayer MoS_2 from first principles," Phys. Rev. B **91**, 125304 (2015).
[25]Z. Yu, Y. Pan, Y. Shen, Z. Wang, Z. Ong, T. Xu, R. Xin, L. Pan, B. Wang, L. Sun, J. Wang, G. Zhang, Y. W. Zhang, Y. Shi, and X. Wang, "Towards intrinsic charge transport in monolayer molybdenum disulfide by defect and interface engineering," Nat. Commun. **5**, 5290 (2014).
[26]S. KC, R. C. Longo, R. Addou, R. M. Wallace, and K. Cho, "Impact of intrinsic atomic defects on the electronic structure of MoS_2 monolayers," Nanotechnology **25**, 375703 (2014).
[27]A. T. Garcia-Esparza, S. Park, H. Abroshan, O. A. P. Mellone, J. Vinson, B. Abraham, T. R. Kim, D. Nordlund, A. Gallo, R. Alonso-Mori, X. Zheng, and D. Sokaras, "Local structure of sulfur vacancies on the basal plane of monolayer MoS_2," ACS Nano **16**, 6725 (2022).
[28]X. Zhang, H. Wang, J. Liu, M. Zhao, and F. Liu, "Topological superconductivity of line defects in transition metal dichalcogenides," Phys. Rev. B **108**, 144101 (2023).
[29]M. Tang, W. Yin, S. Liu, H. Yu, Y. He, Y. Cai, and L. Wang, "Sulfur line vacancies in MoS_2 for catalytic hydrogen evolution reaction," Crystals **12**, 1218 (2022).
[30]Y. Zhao, M. T. Tang, S. Wu, J. Geng, Z. Han, K. Chan, P. Gao, and H. Li, "Rational design of stable sulfur vacancies in molybdenum disulfide for hydrogen evolution," J. Catal. **382**, 320 (2020).
[31]Q. Chen, H. Li, S. Zhou, W. Xu, J. Chen, H. Sawada, C. S. Allen, A. I. Kirkland, J. C. Grossman, and J. H. Warner, "Ultralong 1D vacancy channels for rapid atomic migration during 2D void formation in monolayer MoS_2," ACS Nano **12**, 7721 (2018).
[32]H.-P. Komsa, S. Kurasch, O. Lehtinen, U. Kaiser, and A. V. Krasheninnikov, "From point to extended defects in two-dimensional MoS_2: Evolution of atomic structure under electron irradiation," Phys. Rev. B **88**, 035301 (2013).
[33]D. Nečas and P. Klapetek, "Gwyddion: An open-source software for SPM data analysis," Cent. Eur. J. Phys. **10**, 181 (2012).
[34]G. Kresse and D. Joubert, "From ultrasoft pseudopotentials to the projector augmented-wave method," Phys. Rev. B **59**, 1758 (1999).
[35]P. E. Blöchl, "Projector augmented-wave method," Phys. Rev. B **50**, 17953 (1994).
[36]J. P. Perdew, K. Burke, and M. Ernzerhof, "Generalized gradient approximation made simple," Phys. Rev. Lett. **77**, 3865 (1996).
[37]M. Methfessel and A. T. Paxton, "High-precision sampling for Brillouin-zone integration in metals," Phys. Rev. B **40**, 3616 (1989).
[38]MedeA-2.22. Materials Design, Inc., San Diego, CA, USA (2017).
[39]J. Towns, T. Cockerill, M. Dahan, I. Foster, K. Gaither, A. Grimshaw, V. Hazlewood, S. Lathrop, D. Lifka, G. D. Peterson, R. Roskies, J. R. Scott, and N. Wilkins-Diehr, "XSEDE: Accelerating scientific discovery," Comput. Sci. Eng. **16**, 62 (2014).
[40]C.-P. Lu, G. Li, J. Mao, L.-M. Wang, and E. Y. Andrei, "Bandgap, mid-gap states, and gating effects in MoS_2," Nano Lett. **14**, 4628 (2014).
[41]A. J. Stollenwerk, A. O'Shea, E. Wolter, M. W. Roth, L. H. Strauss, and T. E. Kidd, "Emergence of long range one-dimensional nanostructures in a disordered two-dimensional system: Mn-doped $Ti_{1+\delta}S_2$," J. Phys. Chem. C **116**, 764 (2012).
[42]S. Baik, Y. Koo, and W. Choi, "Decreased n-type behavior of monolayer MoS_2 crystals annealed in sulfur atmosphere," Curr. Appl. Phys. **42**, 38 (2022).